Available online at www.sciencedirect.com
ScienceDirect
Journal of Sound and Vibration 297 (2006) 578–594
JOURNAL OF SOUND AND VIBRATION
www.elsevier.com/locate/jsvi

Control of friction driven oscillation by time-delayed state feedback

J. Das, A.K. Mallik*

Department of Mechanical Engineering, Indian Institute of Technology Kanpur 208016, India

Received 22 June 2005; received in revised form 25 January 2006; accepted 10 April 2006
Available online 19 June 2006

Abstract

An experimental set-up is designed and fabricated to yield a single degree-of-freedom friction-driven oscillator. Self-excited limit cycles obtained experimentally are used to determine the numerical values of the parameters that appear in the mathematical model under pure slip condition. Then the control of the limit cycle using a time-delayed displacement feedback is investigated. The same system under harmonic excitation is also considered. A PD control system with identical time delay in the displacement and velocity feedback is analysed. Only the primary harmonic entrainment region is investigated. Both the best and worst time delays are determined. Stability and bifurcation conditions are discussed. Numerical results are used to verify the analytical results obtained by using the method of multiple time scales and a parametric investigation is included. The proper choice of time delay, which depends on the model parameters, is crucial. It is shown that with appropriate choices of time delay and gain factors, both the limit cycle and the steady-state forced amplitude can be controlled; no time delay or inappropriate time delay can enhance the vibration level.

1. Introduction

Friction driven oscillation, a type of self-excited oscillation, is a serious problem in many engineering systems. The friction force acting on the system provides the energy needed to maintain these vibrations. The nature of the friction force, dependent on the relative (slip) velocity, time, temperature, material properties, geometry and roughness of sliding surfaces, normal load etc., is really complex [1–6]. Ibrahim and co-workers [1–3] have considered linear and nonlinear phenomenological models of interfacial friction forces between sliding surfaces and between a rotating disc and a pin. Modelling of friction force and friction oscillators has attracted the attention of both physicists and engineers [7,8]. In the nonlinear model under pure slip condition, the friction force appears as a polynomial function of slip velocity having terms up to order three. Control of self-excited oscillations, in general, is under investigation for quite sometime [9].

Nonlinear difference-differential equations involving time delays have been studied in various engineering and scientific fields. In real-life applications, time delay cannot be avoided in the feedback line of any active vibration control system. Active vibration suppression with time-delayed feedback is a fast growing field in the

*Corresponding author. Tel.: +91 512 5907098; fax: +91 512 597995.
E-mail address: akmallik@iitk.ac.in (A.K. Mallik).

0022-460X/$ - see front matter © 2006 Elsevier Ltd. All rights reserved.
doi:10.1016/j.jsv.2006.04.013

area of vibration control [10–12]. Maccari [13,14] investigated the primary resonance of an excited Van der Pol oscillator and a cantilever beam under state feedback control with a time delay. Energy considerations were used to study the existence and characteristics of limit cycles corresponding to a two-period modulated motion for the Van der Pol oscillator. Maccari [15] also considered a parametrically excited Van der Pol oscillator with a time-delay state feedback. Plaut and Hsieh [16] used the method of multiple time scales to study a forced nonlinear system with time delay in the damping term. Six different resonance conditions including primary, subharmonic, superharmonic and parametric resonance were considered. Heckl and Abrahams [17] discussed active control of a friction driven oscillator. The stability analysis of the controlled system was carried out by considering complex eigenfrequencies and energy balance.

In this paper, experimental results are used for determining the numerical values of the parameters to be used in the mathematical model representing a friction driven oscillator consisting of a spring–mass combination placed on a belt moving along its length at a constant speed. The movement of the mass is restrained in all directions other than that of the moving belt by a linear bearing. A nonlinear but smooth variation of the friction force under pure slip condition is assumed. The equation of motion is derived by expanding the friction force in a Taylor series with slip velocity as the independent variable. Terms up to third order are retained. With the first derivative negative, the vibration grows and attains a limit cycle. This limit cycle is obtained experimentally and is used to obtain the numerical values of the terms appearing in the Taylor series. A control force proportional to the time-delayed displacement of the mass is assumed.

The same mathematical model is then considered with a harmonic force excitation on the block. A PD control system with identical time delay in both the displacement and velocity feedback signals are considered for possible control of the steady state oscillation amplitude. Only the primary resonance (harmonic frequency entrainment [18]) is investigated.

The perturbation technique based on multiple time scales [19,20] is employed for analytical treatment of both the limit cycle and the forced vibration response with time-delay state feedback. A second-order expansion is required for the friction model considered in this paper. Two slow flow equations for the amplitude and phase of the oscillators are derived. In the forced case with multiple solutions, the conditions for stability and bifurcations are reported. Analytical results are compared with those obtained by numerical integration of the delay differential equations using MATLAB. Finally the results of parametric investigation [21], pointing out the best and worst time delays, are reported.

2. Mathematical model

The free body diagram of a block of mass m, placed on a moving belt and constrained by a spring of stiffness k, is shown in Fig. 1. The inertial coordinate Z of the mass is chosen in such a way that $Z = 0$ corresponds to the unstretched state of the spring. The friction force F is a function of the slip velocity $(v_0 - \dot{Z})$ where the dot denotes differentiation with respect to time t. The equation of motion for the mass can be written as

$$m\ddot{Z} + kZ = F(v_0 - \dot{Z}). \tag{1}$$

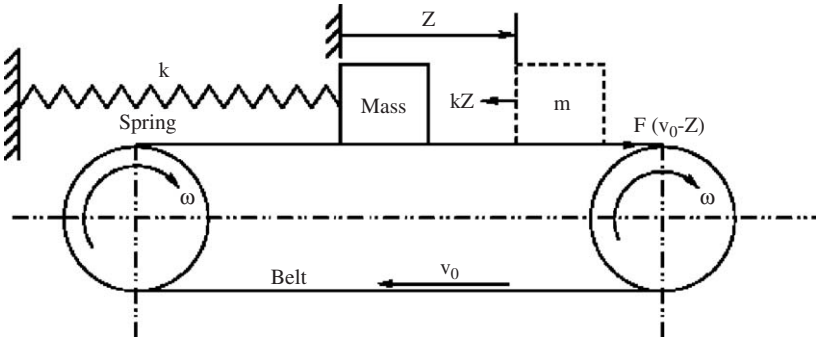

Fig. 1. Schematic diagram of a mass–spring system on a moving belt as a model of friction-driven oscillation.

It is convenient to introduce a new variable X as

$$X(t) = Z(t) - \frac{F(v_0)}{k}, \tag{2}$$

when Eq. (1) can be rewritten as

$$m\ddot{X} + kX = F(v_0 - \dot{X}) - F(v_0). \tag{3}$$

Expanding the first term on the RHS of Eq. (3) in a Taylor series and retaining up to the third derivative one gets

$$m\ddot{X} + kX + F'\dot{X} = \tfrac{1}{2}F''\dot{X}^2 - \tfrac{1}{6}F'''\dot{X}^3, \tag{4}$$

where the prime on F denotes derivative of F evaluated at v_0. Now Eq. (4) is written in the following nondimensional form:

$$x'' + x + \alpha x' - \beta x'^2 + \gamma x'^3 = 0, \tag{5}$$

where

$$\omega = \sqrt{(k/m)},\ \ \tau = \omega t,\ \ \alpha = \frac{F'}{\sqrt{mk}},\ \ \beta = \frac{F(v_0)}{2mk}F'',\ \ \gamma = \frac{F^2(v_0)}{6(mk)^{3/2}}F''',\ \ x = \frac{X}{F(v_0)/k}$$

and the primes on x denote differentiation with respect to τ.

The approximate amplitude of the limit cycle of Eq. (5) can be obtained by the energy balance method [22]. Towards this end, one writes

$$x = \rho \sin \tau$$

and gets

$$\rho = \sqrt{-\frac{4\alpha}{3\gamma}}. \tag{6}$$

For the system under consideration $\alpha < 0$ and $\gamma > 0$ At this level of approximation the asymmetric coefficient β does not play any role.

3. Experimental set-up

For experimental investigation of the friction driven oscillator, a single degree-of-freedom oscillator set-up is fabricated. This consists of a mild steel block (1) placed on a rough leather belt (2). Numbers (1), (2) etc. are marked in Fig. 2 which shows two views of the set-up. The block is attached to a rigid fixed support through a coil spring (3). The mass of the block is 272 g. And the stiffness of the spring is 430 N/m. Self-excitation is provided by moving the belt at a constant speed. The belt moves over a pair of pulleys (4), one of which is driven by a single phase induction motor (5) rotating at its rated speed of 1440 rev/min. The pulley shafts are mounted in two pillow blocks standard ball bearings in a cast iron housing (6). Due to continuous operation of the system and climatic changes, the length of the belt may change causing sag of the contact surface (with the block). To avoid this sag, an idler pulley (7) is mounted on the slack side of the belt. This ensures good contact between the moving belt and the block. In order to provide free rotation and vertical adjustment to the idler pulley, two brass bushes (8) are used which can slide through a smooth rectangular pipe (9). The movement of the oscillating block only along the direction of belt movement is ensured by mounting the block on a linear motion (LM) bearing. The LM block (10) is of negligible friction. The rails (11) of the LM bearing are attached to a square cross-section pipe (12) of high bending rigidity. Total movable mass, including the effective one-third mass of the spring, is 303 g. Two vertical end stands (13) are used for overall vertical adjustment of the assembly. The whole assembly is mounted on a heavy base (14) having four legs. The oscillation of the block is measured by an accelerometer, the output signal of which is fed to a FFT analyzer via a charge amplifier. The displacement signal and the associated power spectrum are finally measured.

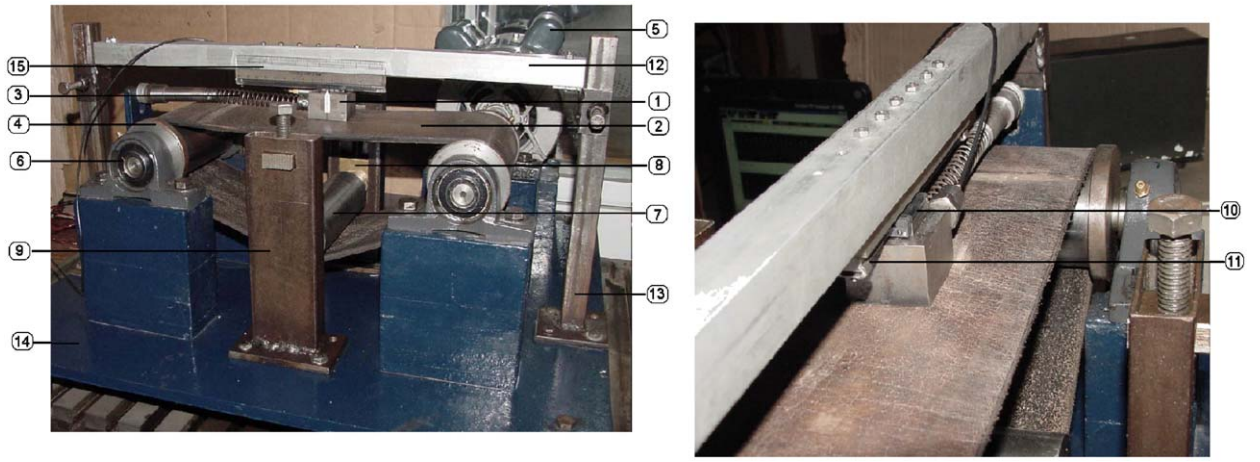

Fig. 2. Experimental set-up: (1) mass, (2) belt, (3) spring, (4) pulleys, (5) single phase induction motor, (6) pillow blocks standards ball bearings, (7) idler pulley, (8) brass bush, (9) rectangular pipe, (10) LM block, (11) LM rail, (12) squared section pipe, (13) end stands, (14) base, (15) scale.

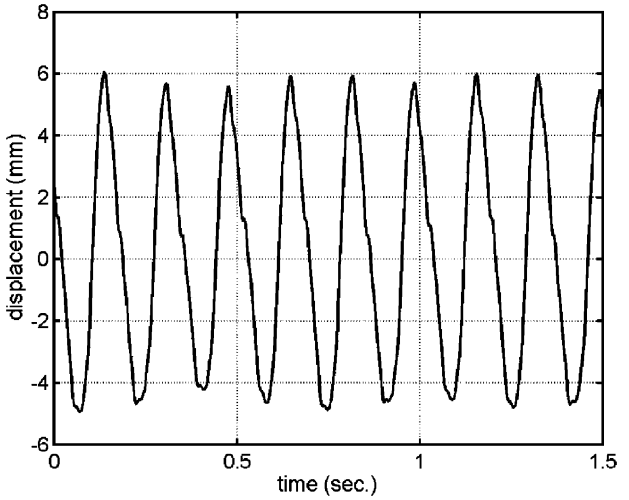

Fig. 3. Steady-state response of the oscillator.

4. Determination of friction model parameters

In order to determine the friction model parameters, i.e., the values of α, β and γ appearing in Eq. (5), a series of free vibration tests is carried out. It is observed that on starting the driving motor, the block starts oscillating with a large amplitude and then settles into a steady-state periodic motion (limit cycle). This steady-state oscillation occurs around a mean position where the spring is stretched by 10.5 mm. Typical time response and the associated power spectrum are shown in Figs. 3 and 4, respectively. It may be noted that the power spectrum exhibits some high-frequency content. Furthermore, this relaxation type oscillation is seen to occur with different maximum values on either side of the zero level and also the time taken in moving from the negative peak to the positive peak is different from that for moving from the positive peak to the negative peak.

Now, Eq. (5) is integrated numerically with different combinations of α, β and γ with different initial conditions. Towards this end, **dde23** numerical integrator of MATLAB 6.5 is used. Once the steady state is reached, the values of peak-to-peak displacement, shift of the zero level and the time intervals with positive and negative velocity in a cycle are compared with those obtained experimentally. This procedure led to the

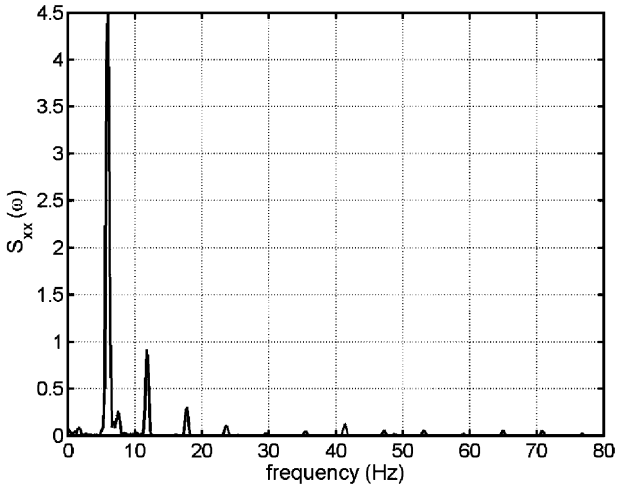

Fig. 4. Power spectrum of the response.

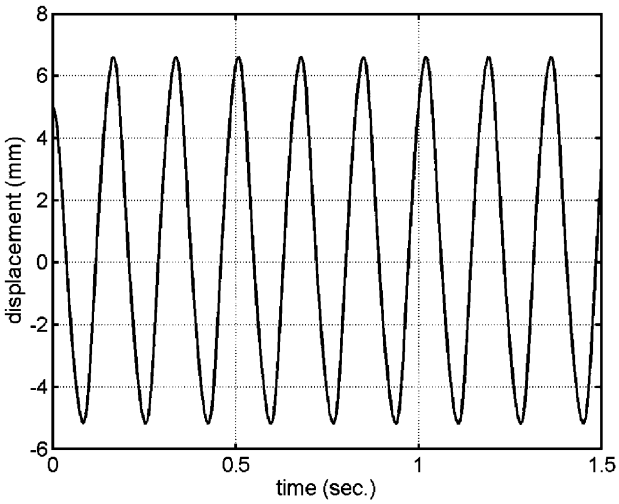

Fig. 5. Time–displacement curve obtained numerically.

following set of values:

$$\alpha = -1.16, \quad \beta = 0.56, \quad \gamma = 5.65.$$

The numerically obtained steady-state time response and the associated power spectrum are shown in Figs. 5 and 6, respectively. These figures are seen to be reasonably close to those obtained experimentally (Figs. 3 and 4). With above values of the parameters, Eq. (6) yields peak-to-peak displacement (2ρ) as 10.5 mm, which is quite acceptable since Eq. (6) does not reflect the effect of β. This value is about 10% less than what is shown in Figs. 3 and 5. Here and onwards, unless otherwise stated, the above values of the parameters are used for all numerical results.

5. Active control of limit cycle

To control the limit cycle of the friction driven oscillator, a control force, f_c, proportional to the displacement of the block with a time delay is assumed. Thus

$$f_c = AX(t - H), \tag{7}$$

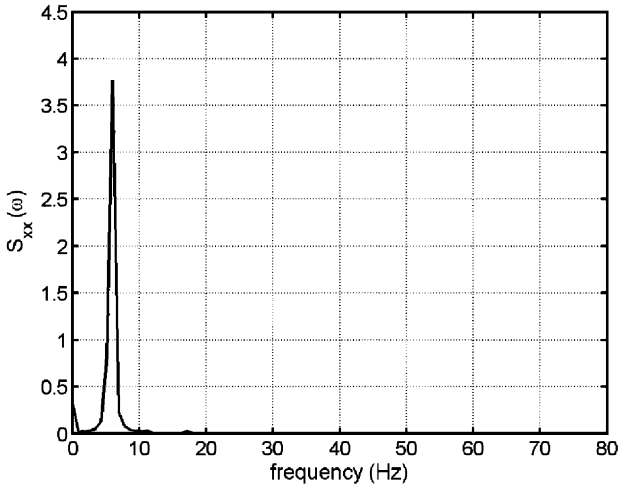

Fig. 6. Power spectrum obtained numerically.

where A is the proportional gain and H is the time delay. The signal X can be obtained by integrating twice the accelerometer signal. With the control force in action, the nondimensional equation of motion of the oscillator can be written as

$$x'' + x + \alpha x' - \beta x'^2 + \gamma x'^3 = g_d x(\tau - h), \tag{8}$$

where $h = \omega H$, $g_d = A/k$ and all other symbols are explained after Eq. (5).

5.1. Analytical method

To apply the method of multiple time scales, Eq. (8) is recast in the following form:

$$x''(\tau) + x(\tau) + \varepsilon^2 \alpha x'(\tau) - \varepsilon \beta x'^2(\tau) + \varepsilon^2 \gamma x'^3(\tau) = \varepsilon^2 g_d x(\tau - h), \tag{9}$$

with $0 < \varepsilon \ll 1$. In Eq. (9), the damping, nonlinearity, proportional feedback gain are assumed to be small. The solution of Eq. (9) can be written in the following form:

$$x(\tau;\varepsilon) = x_0(T_0, T_1, T_2 \ldots) + \varepsilon x_1(T_0, T_1, T_2, \ldots) + \varepsilon^2 x_2(T_0, T_1, T_2, \ldots) + \cdots \tag{10}$$

where $T_n = \varepsilon^n \tau$, $n = 0, 1, 2, \ldots$.

Substituting Eq. (10) into Eq. (9) and equating the coefficient of ε^0, ε^1, and ε^2, on the both sides, one obtains

$$D_0^2 x_0 + x_0 = 0, \tag{11}$$

$$D_0^2 x_1 + x_1 = -2D_0 D_1 x_0 + \beta (D_0 x_0)^2, \tag{12}$$

$$\begin{aligned} D_0^2 x_2 + x_2 = & -2D_0 D_1 x_1 - D_1^2 x_0 - 2D_0 D_2 x_0 - \alpha D_0 x_0 + 2\beta D_0 x_0 (D_0 x_1 + D_1 x_0) \\ & - \gamma (D_0 x_0)^3 + g_d x_0(\tau - h), \end{aligned} \tag{13}$$

where $D_n = \partial/\partial T_n$, $n = 0, 1, 2, \ldots$.

The solution of Eq. (11) can be written as

$$x_0 = A_1(T_1, T_2) \exp(\mathrm{i} T_0) + \bar{A}_1(T_1, T_2) \exp(-\mathrm{i} T_0) \tag{14}$$

and Eq. (12) becomes

$$D_0^2 x_1 + x_1 = -2\mathrm{i} D_1 A_1 \exp(\mathrm{i} T_0) - \beta A_1^2 \exp(2\mathrm{i} T_0) + \beta A_1 \bar{A}_1 + \mathrm{cc}, \tag{15}$$

where A_1 is an unknown complex function and $\bar{A}_1$ is the complex conjugate of A_1. cc denotes the complex conjugate of the preceding terms. To eliminate the secular term from $x_1, D_1 A_1 = 0$, so that $A_1 = A_1(T_2)$.

Hence the solution of Eq. (15) becomes

$$x_1 = \tfrac{1}{3}\beta A_1^2 \exp(2\mathrm{i}T_0) + \tfrac{1}{3}\beta \bar{A}_1^2 \exp(-2\mathrm{i}T_0) + 2\beta A_1 \bar{A}_1. \tag{16}$$

With the use of Eqs. (14) and (16) the secular terms will be eliminated from the solution x_2 of Eq. (13) if

$$-2\mathrm{i}D_2 A_1 - \mathrm{i}\alpha A_1 + \frac{4}{3}\beta^2 A_1^2 \bar{A}_1 - 3\mathrm{i}\gamma A_1^2 \bar{A}_1 + g_d A_1 \exp(-\mathrm{i}h) = 0. \tag{17}$$

It is convenient to put A_1 in the polar form

$$A_1(T_2) = \tfrac{1}{2}\rho(T_2)\exp(\mathrm{i}\vartheta(T_2)), \tag{18}$$

where ρ and ϑ are real. Substituting Eq. (18) into Eq. (17), and separating the real and imaginary parts, one obtains

$$\rho' + \rho\left(\frac{\alpha}{2} + \frac{3}{8}\gamma\rho^2 + \frac{g_d}{2}\sin(h)\right) = 0 \tag{19}$$

and

$$\rho\vartheta' + \rho\left(\frac{1}{6}\beta^2\rho^2 + \frac{g_d}{2}\cos(h)\right) = 0, \tag{20}$$

where primes denote derivatives with respect to T_2.

For steady-state amplitude of the limit cycle, putting $\rho' = 0$, one gets

$$\rho = \sqrt{-\frac{4}{3\gamma}\left(\alpha + g_d \sin(h)\right)}. \tag{21}$$

From Eq. (20), one gets

$$\vartheta' = -\frac{1}{6}\beta^2\rho^2 - \frac{g_d}{2}\cos(h), \tag{22}$$

$$\text{or,} \quad \vartheta = -\left(\frac{1}{6}\beta^2\rho^2 + \frac{g_d}{2}\cos(h)\right)T_2. \tag{23}$$

Thus the periodic solution turns out to be of the form

$$x(\tau) = \rho \cos\left(1 + \varepsilon^2\vartheta\right)\tau + O(\varepsilon), \tag{24}$$

where ρ and ϑ are given by Eqs. (21) and (23), respectively.

It may be pointed out that at this order of approximation, the amplitudes of the limit cycles of the uncontrolled system ($g_d = 0$) and the controlled system with no time delay ($h = 0$) are same (see Eq. (21)) and equal to that given by Eq. (6). Of course, the time period of the limit cycles of these two systems are different. Furthermore, from Eq. (21), it is obvious that the best (for minimum amplitude) and worst (for maximum amplitude) time delays are given, respectively, by $h_{\min} = \pi/2$ and $h_{\max} = 3\pi/2$. Substituting the numerical values with $g_d = 0.28$, one gets $\rho_{\min} = 0.456$ and $\rho_{\max} = 0.583$, where as the limit cycle amplitude of the uncontrolled system is 0.523. The possibility of better control with increasing gain (up to some limit) is also obvious from Eq. (21).

5.2. Numerical results

Eq. (8) is numerically integrated with different initial conditions for various values of g_d and h until the steady state is reached to generate a limit cycle. Detailed numerical studies [21] reveal that the choice of the time-delay parameter h is crucial for effective control of the size of the limit cycle. For this purpose, with the parameter values used, the time delay should lie in the range $(2\pi/7) \leqslant h \leqslant (6\pi/7)$. If the value of h lies in the range $(16\pi/9) \leqslant h \leqslant 2\pi$, the control force has an adverse effect of increasing the size of the limit cycle. The best

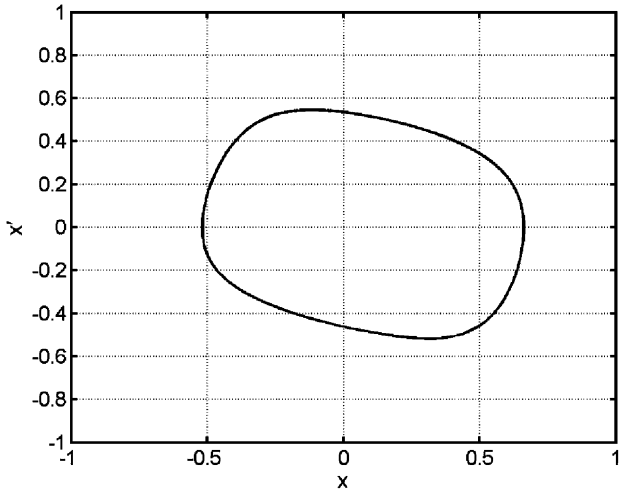

Fig. 7. Limit cycle of the uncontrolled system.

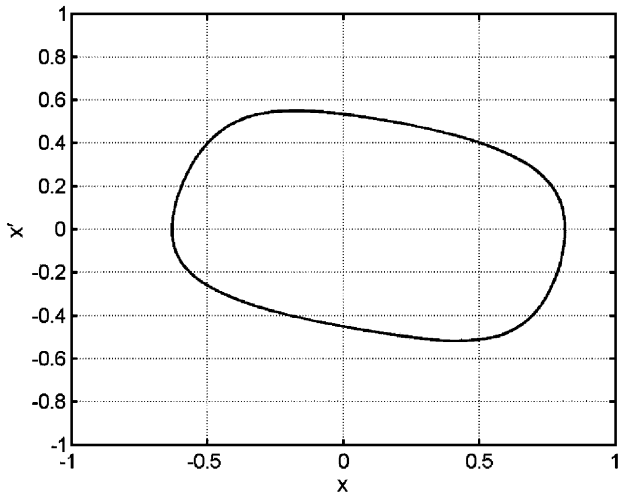

Fig. 8. Limit cycle for the controlled system with $g_d = 0.28$, $h = 0$.

time delay is found to be $h = 2\pi/3$, where as the worst time delay is $h = 17\pi/9$. Figs. 7–10 show the limit cycles obtained with no control and with the same control force (i.e., same value of g_d) having different values of h. It is worth mentioning that with a suitable choice of time delay, increasing the value of the gain parameter g_d from 0.28 to 0.38 was found to be more effective [21]. However, with an unsuitable choice of time delay, increasing the gain parameter was counter-productive and further increased the size of the limit cycle.

The difference between the analytical and numerical results appear to be less for the case of best time delay as compared to that with the worst time delay. Numerical results also clearly indicate that distortion from a harmonic limit cycle, obtained by the approximate analytical method, is least with best time delay ($h = 2\pi/3$) and is quite appreciable for the uncontrolled, controlled with no and worst time delay.

6. Active control of forced response

Let us now consider a control force

$$f_c = AX(t-H) + B\dot{X}(t-H) \tag{25}$$

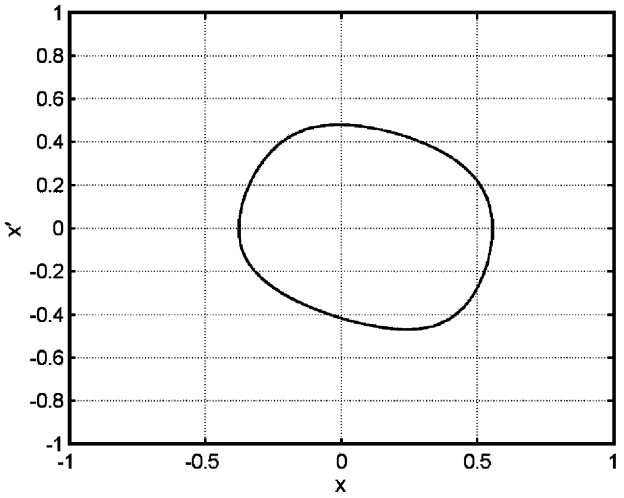

Fig. 9. Limit cycle for $g_d = 0.28$, $h = 2\pi/3$.

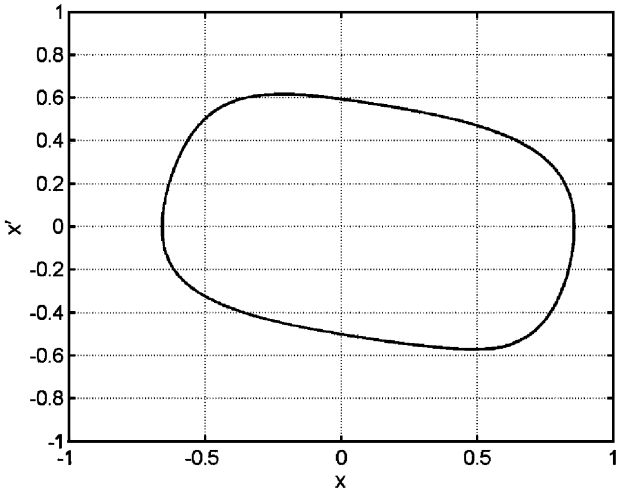

Fig. 10. Limit cycle for $g_d = 0.28$, $h = 17\pi/9$.

acting on the block shown in Fig. 1. Here A and B are the proportional and derivative gains, respectively. Identical time delay H is used for both the signals. Moreover, the block is assumed to be excited by a harmonic force $\Gamma \cos(\bar{\Omega}t)$. Now the equation of motion can be written as

$$m\ddot{X} + kX + AX(t-H) + B\dot{X}(t-H) = -F'\dot{X}(t) + \tfrac{1}{2}F''\dot{X}^2(t) - \tfrac{1}{6}F'''\dot{X}^3(t) + \Gamma\cos(\bar{\Omega}t). \tag{26}$$

In nondimensional form Eq. (26) can be rewritten as

$$x''(\tau) + x(\tau) + \alpha x'(\tau) - \beta x'^2(\tau) + \gamma x'^3(\tau) + g_d x(\tau - h) + g_v x'(\tau - h) = f\cos(\Omega\tau), \tag{27}$$

where $g_v = B/\sqrt{mk}$, $f = \Gamma/F(v_0)$, $\Omega = \bar{\Omega}/\omega$ and all other symbols are defined after Eq. (5).

6.1. Primary harmonic entrainment ($\Omega \approx 1$)

The primary harmonic entrained response and its stability characteristic can be studied by using the method of multiple scales. Towards this end, Eq. (27) is recast in the following form:

$$x''(\tau) + x(\tau) + \varepsilon^2\alpha x'(\tau) - \varepsilon\beta x'^2(\tau) + \varepsilon^2\gamma x'^3(\tau) + \varepsilon^2 g_d x(\tau - h) + \varepsilon^2 g_v x'(\tau - h) = \varepsilon^2 f\ \cos(\Omega\tau), \tag{28}$$

with $0 < \varepsilon \ll 1$. In Eq. (28), the damping, non linearity, feedback gains and excitation terms all are assumed to be small. The solution of Eq. (28) can be written in the following form:

$$x(\tau;\varepsilon) = x_0(T_0, T_1, T_2 \ldots) + \varepsilon x_1(T_0, T_1, T_2, \ldots) + \varepsilon^2 x_2(T_0, T_1, T_2, \ldots) + \cdots + , \tag{29}$$

where $T_n = \varepsilon^n\tau,\ n = 0, 1, 2, \ldots$.

For the case of primary harmonic entrainment set

$$1 = \Omega + \varepsilon^2\sigma, \tag{30}$$

where σ is the detuning parameter.

Substituting Eq. (29) into Eq. (28) and equating the coefficient of ε^0, ε^1, and ε^2 on the both sides, one obtains

$$D_0^2 x_0 + x_0 = 0, \tag{31}$$

$$D_0^2 x_1 + x_1 = -2D_0D_1x_0 + \beta(D_0x_0)^2, \tag{32}$$

$$\begin{aligned} D_0^2 x_2 + x_2 = & -2D_0D_1x_1 - D_1^2x_0 - 2D_0D_2x_0 - \alpha D_0x_0 + 2\beta D_0x_0(D_0x_1 + D_1x_0) \\ & - \gamma(D_0x_0)^3 - g_d x_0(\tau - h) - g_v D_0x_0(\tau - h) + f\ \cos(\Omega\tau), \end{aligned} \tag{33}$$

where $D_n = \partial/\partial T_n,\ \ n = 0, 1, 2, \ldots$.

The solution of Eq. (31) can be written as

$$x_0 = A_1(T_1, T_2)\exp(\mathrm{i}T_0) + \bar{A}_1(T_1, T_2)\exp(-\mathrm{i}T_0) \tag{34}$$

and Eq. (32) becomes

$$D_0^2 x_1 + x_1 = -2\mathrm{i}D_1A_1\exp(\mathrm{i}T_0) - \beta A_1^2\exp(2\mathrm{i}T_0) + \beta A_1\bar{A}_1 + \mathrm{cc}, \tag{35}$$

where A_1 is an unknown complex function with $\bar{A}_1$ as its complex conjugate and cc denotes the complex conjugate of the preceding terms. To eliminate the secular term from x_1 $D_1A_1 = 0$, so that $A_1 = A_1(T_2)$. Hence the solution of Eq. (35) becomes

$$x_1 = \tfrac{1}{3}\beta A_1^2\exp(2\mathrm{i}T_0) + \tfrac{1}{3}\beta\bar{A}_1^2\exp(-2\mathrm{i}T_0) + 2\beta A_1\bar{A}_1. \tag{36}$$

With the use of Eqs. (34) and (36) the secular terms will be eliminated from the solution x_2 of Eq. (33) if

$$-2\mathrm{i}D_2A_1 - \mathrm{i}\alpha A_1 + \frac{4}{3}\beta^2A_1^2\bar{A}_1 - 3\mathrm{i}\gamma A_1^2\bar{A}_1 - g_dA_1\ \exp(-\mathrm{i}h) - \mathrm{i}g_vA_1\ \exp(-\mathrm{i}h) + \frac{f}{2}\exp(-\mathrm{i}\sigma T_2) = 0. \tag{37}$$

It is convenient to put A_1 in the polar form

$$A_1(T_2) = \tfrac{1}{2}\rho(T_2)\ \exp(\mathrm{i}\vartheta(T_2)), \tag{38}$$

where ρ and ϑ are real. Substituting Eq. (38) into Eq. (37) and separating the real and imaginary parts, one obtains

$$\rho' + \rho\left(\frac{\alpha}{2} + \frac{3}{8}\gamma\rho^2 - \frac{g_d}{2}\sin(h) + \frac{g_v}{2}\cos(h)\right) - \frac{f}{2}\sin(\psi) = 0 \tag{39}$$

and

$$\rho\psi' + \rho\left(\sigma - \frac{1}{6}\beta^2\rho^2 + \frac{g_d}{2}\cos(h) + \frac{g_v}{2}\sin(h)\right) - \frac{f}{2}\cos(\psi) = 0, \tag{40}$$

where primes denote derivatives with respect to T_2 and $\psi = -\sigma T_2 - \vartheta$.

Define,

$$\frac{g_d}{2} = K\ \sin(\varphi) \quad \text{and} \quad \frac{g_v}{2} = K\ \cos(\varphi). \tag{41}$$

Therefore, $K = \frac{1}{2}\sqrt{g_d^2 + g_v^2}$ and $\varphi = \tan^{-1}(g_d/g_v)$.

Substitution of Eq. (41) into Eqs. (39) and (40) yields

$$\rho' + \rho\left(\frac{\alpha}{2} + K\ \cos(\varphi + h)\right) + \frac{3}{8}\gamma\rho^3 - \frac{f}{2}\sin(\psi) = 0, \tag{42}$$

$$\rho\psi' + \rho(\sigma + K\ \sin(\varphi + h)) - \frac{1}{6}\beta^2\rho^3 - \frac{f}{2}\cos(\psi) = 0. \tag{43}$$

The solution to Eq. (28) has the form

$$x(\tau) = \rho\ \cos(\Omega\tau - \psi) + \tfrac{1}{2}\varepsilon\beta\rho^2\left(1 + \tfrac{1}{3}\cos(2\Omega\tau - 2\psi)\right) + O(\varepsilon^2), \tag{44}$$

where ρ and ψ are defined by Eqs (42) and (43).

Steady-state solutions for primary harmonic entrainment are obtained from $\rho' = \psi' = 0$. Elimination of ψ from Eqs. (42) and (43) then leads to

$$\rho^2\left(\left(\frac{\alpha}{2} + \frac{3}{8}\gamma\rho^2 + K\ \cos(\varphi + h)\right)^2 + \left(\sigma - \frac{1}{6}\beta^2\rho^2 + K\ \sin(\varphi + h)\right)^2\right) = \left(\frac{f}{2}\right)^2. \tag{45}$$

The best and worst time delay, corresponding to minimum and maximum response amplitude ρ, can be obtained by differentiating Eq. (45) and setting $\mathrm{d}\rho/\mathrm{d}h = 0$, which yields

$$\tan(\varphi + h) = \frac{2\sigma - \frac{1}{3}\beta^2\rho_0^2}{\alpha + \frac{3}{4}\gamma\rho_0^2}. \tag{46}$$

Now returning to Eq. (45), one notes that there can be one or three real values of the amplitude for a given value of the excitation f. Determining the points of vertical tangencies in the frequency response curves in the usual manner [18], one gets after some algebraic manipulation that three real roots exist in the range $\sigma^- < \sigma < \sigma^+$, where

$$\sigma^{\pm} = \left(\frac{1}{3}\beta^2\rho^2 - K\ \sin(\varphi + h)\right) \pm \sqrt{\begin{array}{l}\left(\frac{1}{36}\beta^4 - \frac{27}{64}\gamma^2\right)\rho^4 - \left(\frac{3}{4}\alpha\gamma + \frac{3}{2}\gamma K\ \cos(\varphi + h)\right)\rho^2 \\ -\frac{\alpha^2}{4} - \alpha K\ \cos(\varphi + h) - K^2\cos^2(\varphi + h).\end{array}} \tag{47}$$

When the expression under the radical sign in the right-hand side of Eq. (47) reduces to zero, this interval shrinks to $\sigma = \left(\frac{1}{3}\beta^2\rho^2 - K\ \sin(\varphi + h)\right)$. This critical forcing amplitude can be calculated from Eq. (45) as

$$f_{\mathrm{crit}}^2 = \frac{48\left(18\gamma \pm \sqrt{16\beta^4 + 81\gamma^2}\right)(\alpha + 2K\ \cos(\varphi + h))}{16\beta^4 - 243\gamma^2}\left(\left(\frac{\alpha}{2} + K\cos(\varphi + h)\right.\right.\left.\left.\right.$$

$$+\frac{9\gamma\left(18\gamma \pm \sqrt{16\beta^4+81\gamma^2}\right)(\alpha+2K\ \cos(\varphi+h))}{2\left(16\beta^4-243\gamma^2\right)}\Bigg)^2$$

$$+\frac{4\beta^4\left(18\gamma \pm \sqrt{16\beta^4+81\gamma^2}\right)^2(\alpha+2K\ \cos(\varphi+h))^2}{(16\beta^4-243\gamma^2)^2}\Bigg). \tag{48}$$

For $f>f_{\text{crit}}$ there is only one solution while $f<f_{\text{crit}}$ there are three.

The frequency response curve is given by

$$\sigma=\frac{1}{6}\beta^2\rho^2-K\ \sin(\varphi+h)\pm\sqrt{\left(\frac{f}{2\rho}\right)^2-\left(\frac{\alpha}{2}+\frac{3}{8}\gamma\rho^2+K\ \cos(\varphi+h)\right)^2}. \tag{49}$$

6.2. Stability analysis

One or three values of the amplitudes obtained in Section 6.1 may or may not be stable.

The stability of the response curve is determined by the eigenvalues of the corresponding Jacobian matrix (**J**) obtained from Eqs. (42) and (43) by superposing small perturbations and linearizing the resulting equations. The eigenvalues are given by

$$\lambda^2-P\lambda+Q=0, \tag{50}$$

where the trace and determinant of the linearized matrix are defined by

$$P=-\left(\alpha+\tfrac{3}{2}\gamma\rho_0^2+2K\ \cos(\varphi+h)\right) \tag{51}$$

and

$$Q=\left(\frac{\alpha}{2}+\frac{9}{8}\gamma\rho_0^2+K\ \cos(\varphi+h)\right)\times\left(\frac{\alpha}{2}+\frac{3}{8}\gamma\rho_0^2+K\ \cos(\varphi+h)\right)$$
$$+\left(\sigma-\frac{1}{6}\beta^2\rho_0^2+K\ \sin(\varphi+h)\right)\times\left(\sigma-\frac{1}{2}\beta^2\rho_0^2+K\ \sin(\varphi+h)\right). \tag{52}$$

A root with positive real part indicates an unstable solution, whereas if the real parts of the eigenvalues are all negative then the steady-state solution is stable. The stability and bifurcation conditions for the periodic solutions are as follows:

Stability conditions:

(i) Stable periodic solutions corresponding to a stable focus are

$$\alpha+\frac{3}{2}\gamma\rho_0^2+2K\cos(\varphi+h)>0, \tag{53}$$

$$\sigma^2+K^2+\frac{\alpha^2}{4}+\left(\frac{1}{12}\beta^4+\frac{27}{64}\gamma^2\right)\rho_0^4+\left(\frac{3}{4}\alpha\gamma-\frac{2}{3}\sigma\beta^2\right)\rho_0^2+\left(\alpha+\frac{3}{2}\gamma\rho_0^2\right)K\ \cos(\varphi+h)$$
$$+\left(2\sigma-\frac{2}{3}\beta^2\rho_0^2\right)K\ \sin(\varphi+h)>0. \tag{54}$$

(ii) Unstable periodic solutions corresponding to an unstable focus are

$$\alpha+\tfrac{3}{2}\gamma\rho_0^2+2K\ \cos(\varphi+h)<0, \tag{55}$$

$$\sigma^2 + K^2 + \frac{\alpha^2}{4} + \left(\frac{1}{12}\beta^4 + \frac{27}{64}\gamma^2\right)\rho_0^4 + \left(\frac{3}{4}\alpha\gamma - \frac{2}{3}\sigma\beta^2\right)\rho_0^2 + \left(\alpha + \frac{3}{2}\gamma\rho_0^2\right)K\ \cos(\varphi + h) + \left(2\sigma - \frac{2}{3}\beta^2\rho_0^2\right)K\ \sin(\varphi + h) > 0. \tag{56}$$

(iii) Unstable periodic solutions corresponding to a saddle is

$$\sigma^2 + K^2 + \frac{\alpha^2}{4} + \left(\frac{1}{12}\beta^4 + \frac{27}{64}\gamma^2\right)\rho_0^4 + \left(\frac{3}{4}\alpha\gamma - \frac{2}{3}\sigma\beta^2\right)\rho_0^2 + \left(\alpha + \frac{3}{2}\gamma\rho_0^2\right)K\ \cos(\varphi + h) + \left(2\sigma - \frac{2}{3}\beta^2\rho_0^2\right)K\ \sin(\varphi + h) < 0. \tag{57}$$

Bifurcation conditions:

(i) Hopf bifurcation occurs when

$$\rho_0^2 = -\frac{2}{3\gamma}(\alpha + 2K\ \cos(\varphi + h)) \geqslant 0, \tag{58}$$

$$f^2 = -\frac{1}{6\gamma}(\alpha + 2K\cos(\varphi + h)) \times \left((\alpha + 2K\cos(\varphi + h))^2 + 16\left(\sigma + \frac{\beta^2}{9\gamma}(\alpha + 2K\cos(\varphi + h)) + K\sin(\varphi + h)\right)^2\right)$$

and

$$\sigma^2 + K^2 + \frac{\alpha^2}{4} + \frac{4}{9\gamma^2}\left(\frac{1}{12}\beta^4 + \frac{27}{64}\gamma^2\right)(\alpha + 2K\cos(\varphi + h))^2 - \frac{2}{3\gamma}\left(\frac{3}{4}\alpha\gamma - \frac{2}{3}\sigma\beta^2\right)(\alpha + 2K\cos(\varphi + h)) - 2K^2\cos^2(\varphi + h) + \left(2\sigma + \frac{4\beta^2}{9\gamma}(\alpha + 2K\cos(\varphi + h))\right)K\sin(\varphi + h) > 0. \tag{59}$$

Anyhow, the above case should be avoided from the view point of bifurcation control. The feedback should be implemented at least in such a way that $P < 0$ is guaranteed. Under such feedback gains and time-delays, the trace is always negative, and accordingly, at least one of the two eigenvalues will always have a negative part.

(ii) Saddle-node bifurcation will occur

$$\sigma^2 + K^2 + \frac{\alpha^2}{4} + \left(\frac{1}{12}\beta^4 + \frac{27}{64}\gamma^2\right)\rho_0^4 + \left(\frac{3}{4}\alpha\gamma - \frac{2}{3}\sigma\beta^2\right)\rho_0^2 + \left(\alpha + \frac{3}{2}\gamma\rho_0^2\right)K\ \cos(\varphi + h) + \left(2\sigma - \frac{2}{3}\beta^2\rho_0^2\right)K\ \sin(\varphi + h) = 0. \tag{60}$$

For some values of time-delay and feedback gain, the left-hand side of Eq. (60) is positive when no unstable solution exists. The system will not exhibit jump and hysteresis phenomenon. Thus, the appropriate feedback gains and time-delays can enhance the control performance.

6.3. Numerical results and discussion

The steady-state amplitude is also computed by numerically integrating Eq. (28) using **dde23** of MATLAB. Integration is carried out until transients die down and a steady state is reached. For this integration ε is taken as unity with $\Omega = 1 - \sigma$. Integration is carried out with different initial conditions to arrive at the same steady state. The best and worst time delay parameters obtained earlier by analytical method are used.

Unless otherwise stated, the gain factors are taken as $g_d = 0.28$ and $g_v = 0.12$. Using the relevant equations, it was found that for high values of f (>10), both the worst and best time delay parameters are rather insensitive to the value of f and can be taken as $h = 1.95$ and 5.09, respectively [21]. For lower values of f, depending on the value of f, the best time delay parameter varies monotonically from $h = 4.81$ to 5.08, where as the worst time delay parameter varies from $h = 1.81$ to 1.93. Figs. 11 and 12 show the response as a function of the excitation for a given value of the detuning parameter (i.e., at a particular forcing frequency). Fig. 11 shows the results for a low range of excitation amplitude and Fig. 12 for the higher range. In Fig. 11, the dotted lines represent the unstable amplitudes. Both these figures reveal that the control is more effective when

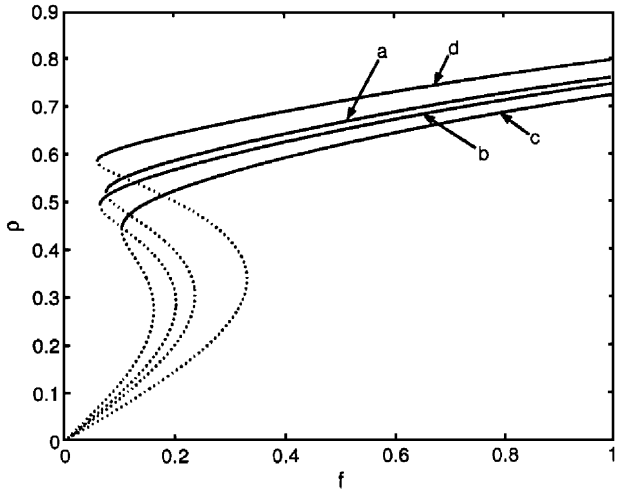

Fig. 11. Excitation-response curves with $g_d = 0.28$, $g_v = 0.12$, $\sigma = -0.06$: (a) uncontrolled; (b) $h = 0$; (c) $h = 4.81$; (d) $h = 1.81$.

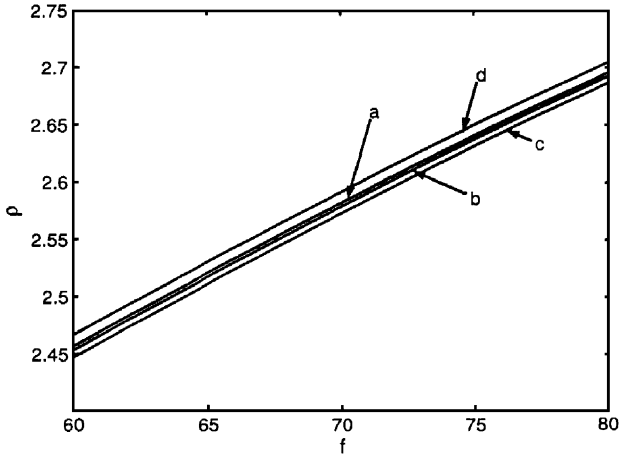

Fig. 12. Excitation-response curves with $g_d = 0.28$, $g_v = 0.12$, $\sigma = -0.06$: (a) uncontrolled; (b) $h = 0$; (c) $h = 5.09$; (d) $h = 1.95$.

the best time delay is used as compared to no time delay. The worst time delay has an adverse effect of increasing the amplitude.

The excitation-response curves shown in Fig. 11 are quite closely reproduced by numerical integration as shown in Fig. 13. Of course, the unstable solutions denoted by dotted lines are not obtained by numerical integration. In Fig. 13, the black squares represent the results obtained by numerical integration. The data for Fig. 13 are same as those for Figs. 11(a)–(d).

The frequency response curves for a given value of the excitation are shown in Fig. 14. The time delay parameter values are same as those given in Fig. 11. Since the best time delay $h = 4.81$ was obtained for $\sigma = -0.06$, the corresponding curve c exhibits minimum response in that frequency range. It should be noted that for this choice of the time delay parameter, the entrained frequency range is also the widest. Fig. 15 shows the variation of the entrainment region with increasing excitation amplitude. All the curves in Fig. 15 correspond to $h = 4.81$. The values of gain parameters are kept the same for Figs. 11–15. From Fig. 15 it is seen that the entrainment region widens with increasing excitation as expected.

Results are presented so far for fixed values of the friction model parameters α, β and γ (as given in Section 4) and also of gain parameters $g_d = 0.28$, $g_v = 0.12$. A detailed parametric study [21] reveals the following facts. With increasing value of $|\alpha|(\alpha<0)$ and decreasing value of γ, the excitation level needed to produce harmonic entrainment hardly changes, but the entrained response is higher. If the value of β increases, the response is less and the frequency response curve becomes asymmetric about $\sigma = 0$. Without any time delay,

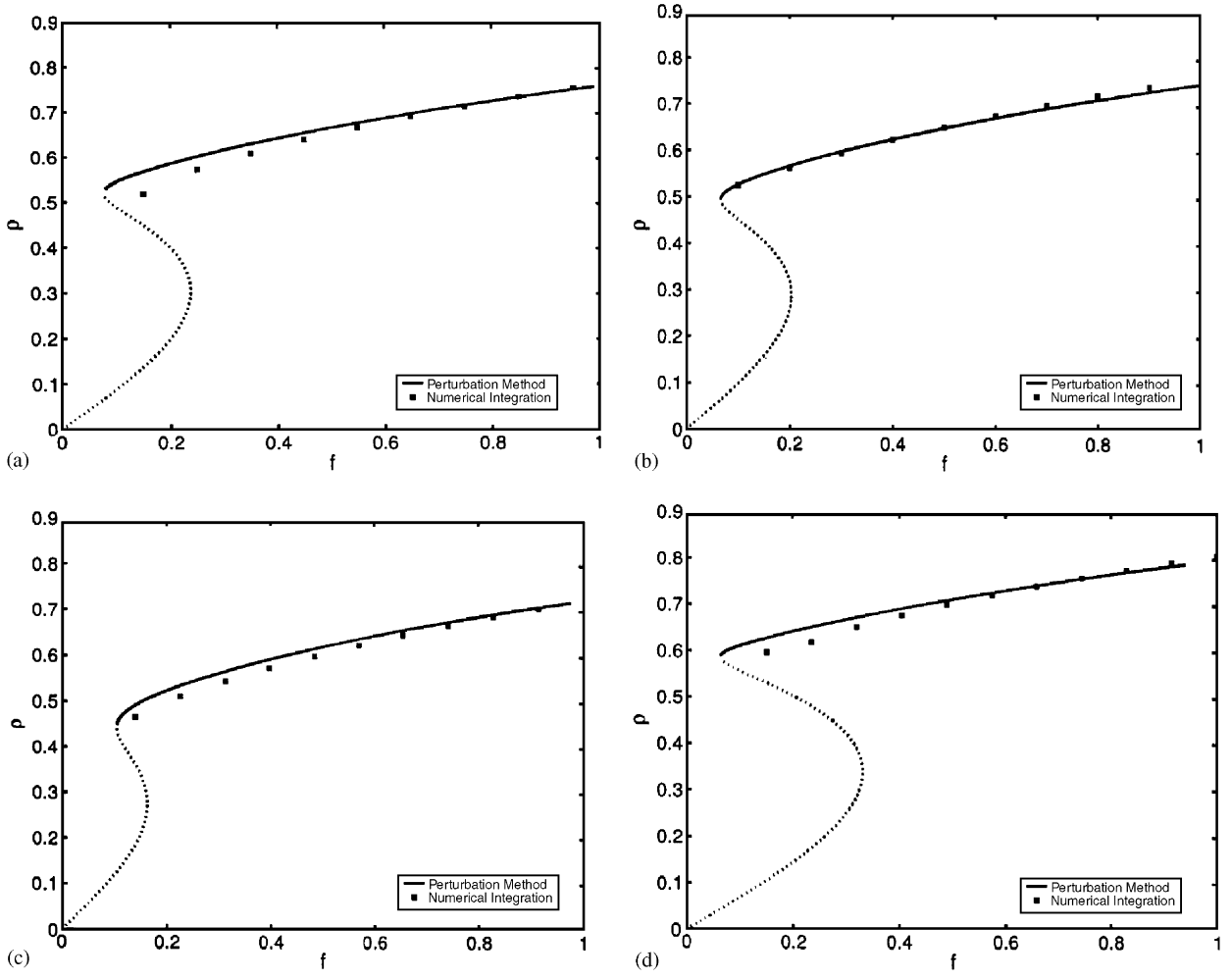

Fig. 13. Comparison of analytical and numerical results.

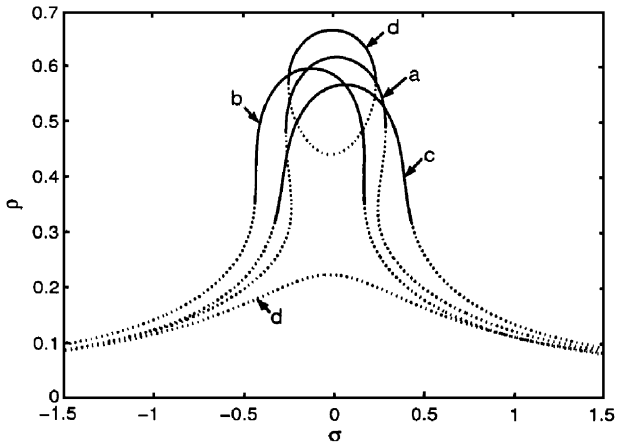

Fig. 14. Frequency response curve. $f = 0.28$, (a) uncontrolled; (b) $h = 0$; (c) $h = 4.81$; (d) $h = 1.81$.

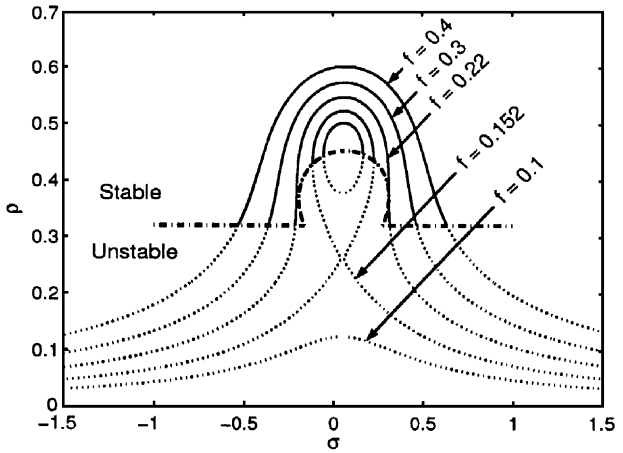

Fig. 15. Harmonic entrainment region with different excitation level and $h = 4.81$.

increasing g_d increases the critical value of the excitation to cause entrainment, but the response of the entrained amplitude hardly changes. With the best time delay, the response is lower with increasing g_d; but with the worst time delay the effect is just opposite. Without any time delay, increase in g_v does not affect the critical excitation level but decreases the response. With best and worst time delays, the effect of g_v is similar to that of g_d.

7. Conclusions

A control force proportional to the displacement can control the limit cycle amplitude of a friction driven oscillator, only if a suitable time delay employed. No time delay or unsuitable time delay may increase the limit cycle amplitude. The proper choice of the amount of delay depends on the friction model parameters, which can be determined experimentally with reasonable accuracy under pure slip condition. Increasing the gain parameter, up to some limit, can help only if a proper time delay is used. Results obtained by using multiple time scale method have been compared with those obtained by direct numerical integration.

The multiple time scale method can be conveniently used for analysing the primary harmonic entrainment region of a forced, friction driven oscillator having identical time delay in the displacement and velocity feedback. Numerical integration validates the results obtained by the multiple time scale method. The choice of the time delay parameter is again crucial; otherwise the response may be adversely affected. The appropriate

choice of the time delay depends also on the level of excitation along with the friction force model parameters. The critical level of excitation needed to cause entrainment depends on various parameters. A high value of the second derivative of the friction force with respect to slip velocity causes asymmetry in the frequency response curve.

Acknowledgement

The authors would like to thank the reviewers for their constructive suggestions on an earlier draft.

References

[1] R.A. Ibrahim, Friction-induced vibration, chatter, squeal, and chaos. Part I: mechanics of contact and friction, *Applied Mechanics Reviews* 47 (7) (1994) 209–226.
[2] R.A. Ibrahim, Friction-induced vibration, chatter, squeal, and chaos. Part II: dynamics and modeling, *Applied Mechanics Reviews* 47 (7) (1994) 227–253.
[3] S.L. Qiao, R.A. Ibrahim, Stochastic dynamics of systems with friction-induced vibration, *Journal of Sound and Vibration* 223 (1) (1999) 115–140.
[4] A. Guran, F. Feeny, N. Hinrichs, K. Popp, A historical review on dry friction and stick–slip phenomenon, *Applied Mechanics Reviews* 51 (5) (1998) 321–341.
[5] A.J. McMillan, A non-linear friction model for self excited vibrations, *Journal of Sound and vibration* 205 (3) (1997) 323–335.
[6] J.J. Thomsen, Using fast vibrations to quench friction induced oscillations, *Journal of Sound and Vibration* 228 (5) (1999) 1079–1102.
[7] F.J. Elmer, Nonlinear dynamics of dry friction, *Journal of Physics A– Mathematical and General* (30) (1997) 6057–6063.
[8] N. Hinrichs, M. Oestreich, K. Popp, On the modeling of friction oscillators, *Journal of Sound and Vibration* 216 (3) (1998) 435–459.
[9] A. Tondl, *Quenching of Self-excited Vibrations*, Elsevier, Amsterdam, 1991.
[10] R. Sipahi, N. Olgac, Active vibration suppression with time delayed feedback, *Journal of Vibration and Acoustics—Transactions of ASME* (125) (2003) 384–388.
[11] F.M. Atay, Van der Pol oscillator under delayed feedback, *Journal of Sound and Vibration* 218 (2) (1998) 333–339.
[12] J.C. Ji, A.Y.T. Leung, Resonances of a non-linear s.d.o.f. system with two time-delay in linear feedback control,, *Journal of Sound and Vibration* 253 (5) (2002) 985–1000.
[13] A. Maccari, Vibration control for the primary resonance of the Van der pol oscillator by a time delay state feedback, *International Journal of Non-Linear Mechanics* (38) (2003) 123–131.
[14] A. Maccari, Vibration control for the primary resonance of a cantilever beam by a time delay state feedback, *Journal of Sound and Vibration* 259 (2) (2003) 241–251.
[15] A. Maccari, The response of a parametrically excited Van der Pol oscillator to a time-delay state feedback, *Nonlinear Dynamics*, (2001).
[16] R.H. Plaut, J.C. Hsieh, Non-linear structural vibrations involving a time delay in damping, *Journal of Sound and Vibration* 117 (3) (1987) 497–510.
[17] M.A. Heckl, I.D. Abrahams, Active control of friction driven oscillations, *Journal of Sound and Vibration* 193 (1) (1996) 417–426.
[18] C. Hayashi, *Nonlinear Oscillations in Physical Systems*, New York, Mc-Graw Hill Book Co, 1964.
[19] A.H. Nayfeh, D.T. Mook, *Nonlinear Oscillations*, New York, Wiley, 1979.
[20] A.H. Nayfeh, *Introduction to Perturbation Techniques*, New York, Wiley, 1981.
[21] J. Das, Control of Friction Driven Oscillation by Time Delay State Feedback, M. Tech. Thesis, IIT Kanpur, India, 2004.
[22] Y. Panovko, *Elements of the Applied Theory of Elastic Vibration*, Moscow, Mir Publishers, 1971.